
Article:
Hong, B orcid.org/0000-0002-8033-5438, Swithenbank, M orcid.org/0000-0002-6146-1818, Greenall, N orcid.org/0000-0002-7700-0549 et al. (6 more authors) (2018) Low-Loss Asymptotically Single-Mode THz Bragg Fiber Fabricated by Digital Light Processing Rapid Prototyping. IEEE Transactions on Terahertz Science and Technology, 8 (1). pp. 90-99. ISSN 2156-342X

https://doi.org/10.1109/TTHZ.2017.2778047

Low-Loss Asymptotically Single-Mode THz Bragg Fiber Fabricated by Digital Light Processing Rapid Prototyping

Binbin Hong, *Student Member, IEEE*, Matthew Swithenbank, Nicholas Greenall, Roland Clarke, *Member*, IEEE, Nonchanutt Chudpooti, *Student Member, IEEE,* Prayoot Akkaraekthalin, *Member, IEEE*, Nutapong Somjit, *Member, IEEE*, John Cunningham, and Ian Robertson, *Fellow, IEEE*

***Abstract*—In this paper, the design and measurement of a 3D-printed low-loss asymptotically single-mode hollow-core terahertz Bragg fiber is reported, operating across the frequency range from 0.246 to 0.276 THz. The HE_{11} mode is employed as it is the lowest loss propagating mode, with the electromagnetic field concentrated within the air core as a result of the photonic crystal bandgap behavior. The HE_{11} mode also has large loss discrimination compared to its main competing HE_{12} mode. This results in asymptotically single-mode operation of the Bragg fiber, which is verified by extensive simulations based on the actual fabricated Bragg fiber dimensions and measured material parameters. The measured average propagation loss of the Bragg fiber is lower than 5 dB/m over the frequency range from 0.246 to 0.276 THz, which is, to the best of our knowledge, the lowest loss asymptotically single-mode all-dielectric microstructured fiber yet reported in this frequency range, with a minimum loss of 3 dB/m at 0.265 THz.**

***Index Terms*—Bragg fiber, electromagnetic propagation, millimeter wave technology, photonic crystals, three-dimensional printing.**

I. Introduction

TERAHERTZ (THz) radiation is of significant interest to the scientific community due to its characteristic time scale, wavelength, and associated energy scale, and has attracted much recent attention for various applications such as radio astronomy, biomedical sensing, wireless communication, security imaging and non-destructive testing [1]-[4]. However, the development of practical THz systems has proved to be challenging owing to the lack of suitable sources and detectors, along with the high loss of typical transmission media [5]. Low-loss THz waveguides, a crucial component needed to provide interconnects in THz systems, are of great interest, particularly as the power of THz generators and the sensitivity of THz detectors are relatively low.

Over the last few decades, significant steps have been made towards the development of low-loss THz waveguides and fibers, based on both electronic and photonic approaches. As the signal frequency moves deeper into the THz region, the high Ohmic loss of metals and dielectric material absorption make many traditional waveguides and fibers unsuitable for the low-loss long-distance guidance of THz waves [6], [7], including hollow metallic waveguide [8], [9], coaxial cable [10], microstrip [11], coplanar waveguide [12], substrate integrated waveguide [13], [14], and optical fiber [15].

Microstructured air-core, solid-core, and porous-core fibers have been extensively studied in the optical domain [15] and have recently become an active field of interest for the guidance of THz waves [6], [7], [16]-[31]. Amongst these microstructured fibers, some air-core microstructured fibers stand out as particularly promising [16]-[25]. A spider-web porous fiber fabricated by extrusion has been demonstrated with loss better than 35 dB/m between 0.2 and 0.35 THz with a minimum loss of 1.3 dB/m at 0.24 THz, but single-mode operation is not claimed in the work [16]. Using 3D printing technology, a hollow core fiber with a triangular-lattice cladding around an air cylinder was demonstrated operating near 0.105 THz with 30 dB/m propagation loss [17]. A 3D-printed kagome-lattice THz waveguide with average propagation loss of 8.7 dB/m over three antiresonance windows in the frequency range from 0.2 to 1.0 THz has also been presented [18]. In addition, using 3D stereolithography, a hollow core Bragg fiber with propagation loss of 52.1 dB/m at 0.18 THz [19] was recently reported. In 2011, two rolled large air-core Bragg fibers were reported which exhibited propagation losses of 18 dB/m at 0.69 THz and 12 dB/m at 0.82 THz, respectively [20]. Recently, tube-lattice fibers fabricated with a fiber drawing technique have been demonstrated, to guide the electromagnetic (EM) fields in the low-loss air core based on the antiresonance effect [21], [22]. The latest experimental work on a tube-lattice fiber showed that a propagation loss of approximately 5 dB/m in the fundamental transmission window around 0.27 THz had been achieved, and losses of 1 dB/m in higher order transmission windows were

This work has been supported by the China Scholarship Council, the Thailand Research Fund through the TRF Senior Research Scholar Program with Grant No.RTA6080008 and the Royal Golden Jubilee Ph.D. Program with Grant No.PHD/0093/2557.

B. Hong, M. Swithenbank, N. Greenall, R. Clarke, N. Somjit, J. Cunningham, and I. Robertson are with the School of Electronic and Electrical Engineering, University of Leeds, Leeds LS2 9JT. U.K. (email: {elbho, el08m2s, el09ng, R.G.Clarke, N.Somjit, J.E.Cunningham, I.D.Robertson} @leeds.ac.uk)

N. Chudpooti and P. Akkaraekthalin are with the Department of Electrical and Computer Engineering, Faculty of Engineering, King Mongkut's University of Technology North Bangkok, Bangkok 10800, Thailand (email: c.nonchanutt@gmail.com, prayoot@kmutnb.ac.th)

inferred, being too low to measure reliably [22]. However, as a type of anti-resonant fiber, the tube-lattice fiber in [22] supports a high number of modes, especially in higher order transmission windows due to the relatively large core size, resulting in mode-competition problems [32], [33]. Triangular-lattice microstructured fibers fabricated by stacking were shown to guide terahertz waves [23], [24], and a propagation loss less than 0.87 dB/m around 0.77 THz was achieved [23]. These air-core microstructured fibers [23], [24] exhibit relatively low loss as they are able to tightly confine the EM field in the low-loss air core, based on either the photonic bandgap effect [34], [35] or the antiresonance effect [36], [37], but single-mode operation in these microstructured fibers was not claimed. A dielectric-lined hollow cylindrical metallic waveguide is a very promising structure, having achieved propagation loss of 1 dB/m at 2.54 THz [25]. It can enable quasi-single mode propagation by means of efficient coupling, but multimode interference was also reported which caused measurement difficulties. It is well known that single-mode operation is essential for many practical applications and it is the design of a Bragg fiber that can be operated in an asymptotically single-mode pattern with low loss that is addressed in this paper.

Various fabrication techniques, such as drawing [26]-[29], extrusion [16], stacking [23], [24], [31], drilling [26]-[28], [30], molding [29], rolling [19], coating [25], and 3D printing [17], [18], have been used in the fabrication of THz microstructured fibers. As a cost-effective, fast, convenient fabrication technique, 3D printing is able to produce devices accurately with good repeatability, and hence it has attracted much attention for the fabrication of functional THz components, such as waveguides [17], [18], [38], fibers [39], lenses [40], antenna horns [41], and sensors [19]. 3D printing is also ideal for the fabrication of highly porous structures, which is a challenge for other techniques, such as molding, drawing, rolling, and extrusion, owing to the deformation encountered during processing [7].

In this paper, we describe the design, fabrication, and measured performance of an all-dielectric asymptotically single-mode low-loss THz Bragg fiber fabricated by digital light processing rapid prototyping. The material structure of the proposed Bragg fiber, which uses a single dielectric, reduces the complexity of fabrication, while also making the fiber suitable for sensing applications in acidic or high magnetic field environment, which can be problematic for metallized waveguides [8], [9], [25]. We also demonstrate that 3D printing using digital light processing techniques can be used to conveniently and cost-effectively fabricate high-porosity air-core Bragg fibers, which is challenging for other fabrication techniques. The Bragg fiber is designed to have large loss discrimination between the desired HE_{11} mode and other competing modes, so creating a modal-filtering effect while exhibiting strong mode selectivity. Based on our EM simulations, which use measured characteristics for our materials, and the actual geometric parameters of the fabricated Bragg fiber prototype, an asymptotically single-HE_{11}-mode operation was verified, ensuring the low-loss transmission of

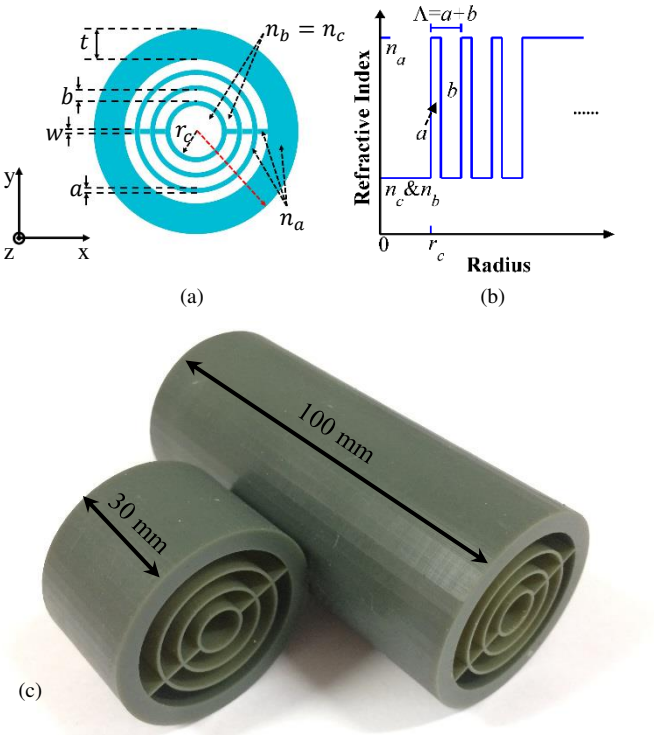

Fig. 1. The proposed Bragg fiber structure: (a) A cross-sectional diagram showing the key design parameters; (b) The radial refractive index profile, taken along the red dashed arrow in (a) starting from the center and going into the edge; (c) A photograph showing the samples with lengths 30 mm and 100 mm. The designed and actual dimensions are listed in TABLE I.

TABLE I
THE DESIGNED AND MEASURED GEOMETRIC PARAMETERS

Parameters	Design (mm)	Measurement (mm)
a	0.652	0.667 ± 0.005
b	3.888	3.877 ± 0.004
r_c	4.742	4.681 ± 0.004
t	4.6	4.544 ± 0.011
w	0.64	0.652 ± 0.009

THz waves since only the desired HE_{11} mode can propagate in the low loss air core. Most importantly, although the loss tangent of the 3D printing material used in this work (EnvisionTEC HTM140) is much higher than other low-loss materials commonly used in the reported THz microstructured fibers, a very low loss asymptotically single-mode Bragg fiber was nonetheless successfully demonstrated.

II. 3D FABRICATION OF THE THZ WAVEGUIDE

Figs. 1(a) and 1(b) show the geometry and the refractive index profile of the proposed Bragg fiber. It comprises an air core ($n_c = 1$), surrounded by periodic concentric dielectric layers of alternating high (n_a) and low (n_b) refractive index materials, the thickness of which are a and b respectively, while r_c is the core radius and $\Lambda = a + b$ is the period of the radial photonic crystal. The outermost layer is a thick protective layer which will absorb any residual EM waves and isolate the fiber from external perturbations. Support bridges are introduced to mechanically maintain the air gaps between dielectric layers. The thicknesses of the outermost layer and the support bridges are represented by t and w, repectively.

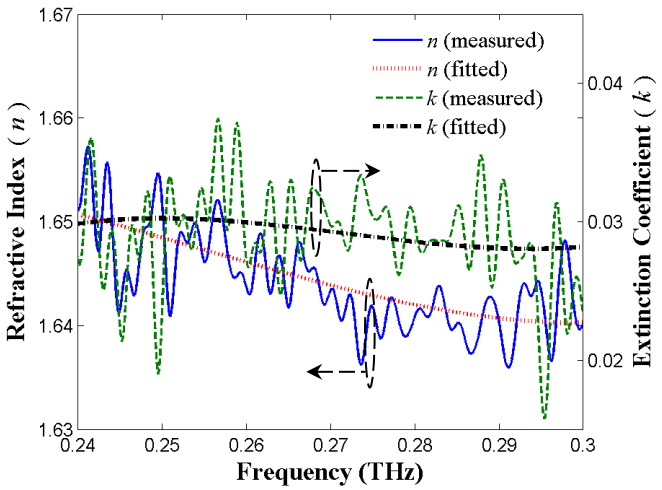

Fig. 2. The complex refractive index of HTM140. The solid blue curve and the dashed green curve represent the refractive index and extinction coefficient of HTM140, respectively, measured using the Keysight commercial free space material characterization platform. The dotted red curve and the dash-dotted black curve are the 3rd-order polynomial regression fitted curves based on the solid blue curve and the dashed green curve, respectively.

In this paper, EnvisionTEC HTM140 photopolymer was the material chosen owing to its high refractive index to provide cladding layers, the outermost protective layer, and the support bridges, while air gaps provided the low refractive index cladding layers ($n_b = n_c = 1$). Fig. 2 shows the complex refractive index of HTM140 over the frequency range from 0.24 to 0.3 THz, measured using the Keysight free-space material characterization platform with a vector network analyser (VNA) and frequency extenders, described in detail in Section IV. The fast ripples in the measurement curves of the complex refractive index of HTM140 are due to residual VNA calibration errors. Two third-order polynomial curves were fitted to the real and imaginary part of the complex refractive index of HTM140, respectively. Compared to other well-known low-loss THz polymers [6], such as Topas, Zeonex, HDPE, and PTFE, the material attenuation of HTM140 is much higher, which is a common limitation of most commercial available photopolymers in 3D printing applications at the time of writing. However, since the EM field in our Bragg fiber is tightly confined and mainly propagates inside the low-loss air core, only a small portion of the EM field is distributed in the periodic cladding material, and thereby the deleterious impact of the relatively high material attenuation of HTM140 is mitigated by our air-core Bragg fiber design.

The geometry of the THz air-core Bragg fiber is listed in TABLE I. The design principle of the proposed Bragg fiber is based on our previous theoretical work [42], which is briefly summarized as follows:

1. As n_a, n_b and n_c are given, the photonic bandgap of the fiber is determined by a and b. Based on the generalized half-wavelength condition presented in our previous theoretical work [42], the values of a and b are chosen to provide a wide photonic bandgap centered around 0.27 THz, which covers the frequency range of interest.
2. Like the classic hollow cylindrical metallic waveguide, the dispersion curves of supported modes in the Bragg fiber are mainly determined by the core radius r_c. Based on the analytical analysis using the transfer-matrix method [42], the value of r_c is carefully chosen to ensure low loss propagation of the desired fundamental HE_{11} mode, as well as a large loss discrimination between the desired mode and its competing modes.
3. Both t and w play a relatively insignificant role in the performance of the proposed Bragg fiber. The outermost layer is designed to be an absorbing layer, so $t > a + b$ can provide good attenuation of signals considering the material as HTM140. The support bridges are perpendicular to the polarization of the HE_{11} mode, and have negligible impact on the loss of the fiber, which will be discussed here in section III.C.

Samples with two different lengths (30 mm and 100 mm, as shown in Fig. 1(c)) were fabricated with the EnvisionTEC Perfactory 3 mini multi-lens 3D printer that uses digital light processing (DLP) rapid prototyping technology. The DLP 3D printer has a fabrication tolerance of 21 μm in the horizontal plane. We found that a minimum dielectric thickness of ~400 μm was needed to achieve good fabrication quality. In order to satisfy this condition, we chose the second-order photonic bandgap as the operating band for the desired fundamental HE_{11} mode, which allows the thickness of the polymer layer to be increased, although it reduces the operating bandwidth [42]. As shown in TABLE I, the fabricated fiber dimensions are in good agreement with the design, within the expected tolerance of the 3D printer's capability.

III. Theoretical Analysis and Simulation

A. Analytical analysis and eigenmode simulation of the ideal Bragg fiber without support bridges

To simplify the complexity of optimizing the design, a Bragg fiber without any support bridges was first investigated, while the impact of the support bridges on the Bragg fiber performance will be discussed in later sections. According to Bloch's theorem in cylindrical coordinates [43], the bandgap diagram of the measured Bragg fiber, with the geometric parameters listed in TABLE I, is as shown in Fig. 3(a). For convenience, the mean value of the complex refractive index of HTM140 over the frequency from 0.24 to 0.3 THz, $n_a = 1.644 + 0.0293i$, was used in the calculation of the bandgap since the slight change over the frequency range of interest has negligible effect on the bandgap shape, verified using our previous theoretical analysis [42]. However, all other analytical results and numerical simulations use the measured and fitted frequency-dependent complex refractive index of HTM140. The black regions represent the bandpass region for TE/HE modes, where the wave can propagate through the periodic cladding layers and is not confined in the fiber. The combined black plus grey regions show the bandpass region for the TM/EH modes. In contrast, the white and grey combined areas indicate the bandstop regions, or electromagnetic bandgaps, for the TE/HE modes: in this case, the wave cannot pass through

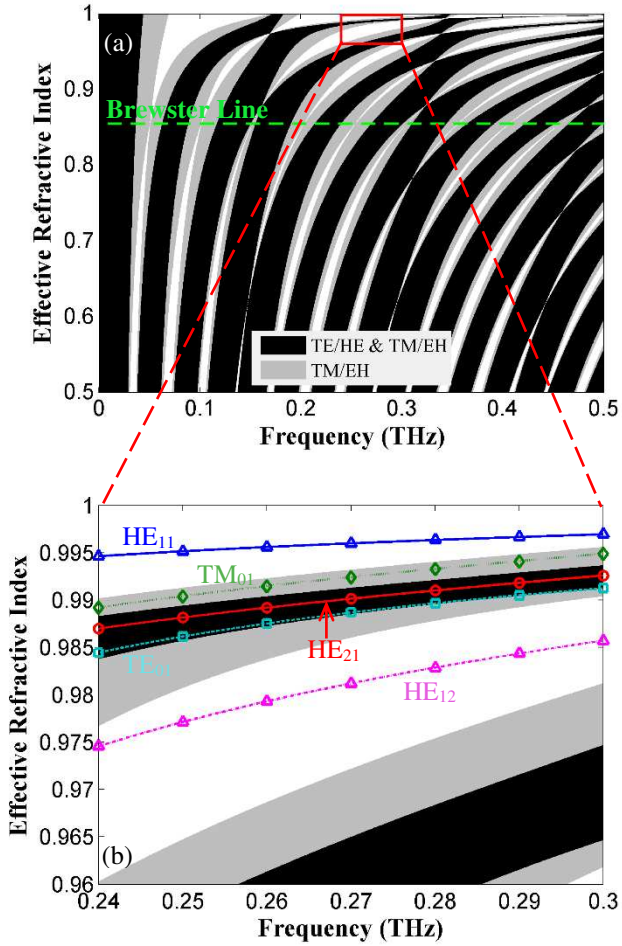

Fig. 3. Bandgap and dispersion curves of the ideal Bragg fiber. (a) Global view of the bandgap behaviour. The black regions represent the bandpass region for TE/HE modes while the black plus grey combined regions are for the TM/EH modes. The dashed green line is the Brewster line. The red box designates the operating parameter range of interest for the designed THz Bragg fiber and is expanded in (b). (b) The bandgap and dispersion curves. The blue solid line, green dotted line, red solid line, cyan dashed line, and magenta dash-dotted line are the analytical dispersion curves for the HE11, TM01, HE21, TE01, and HE12 modes, respectively, calculated using the transfer matrix method. The corresponding colored markers are simulation results obtained from COMSOL.

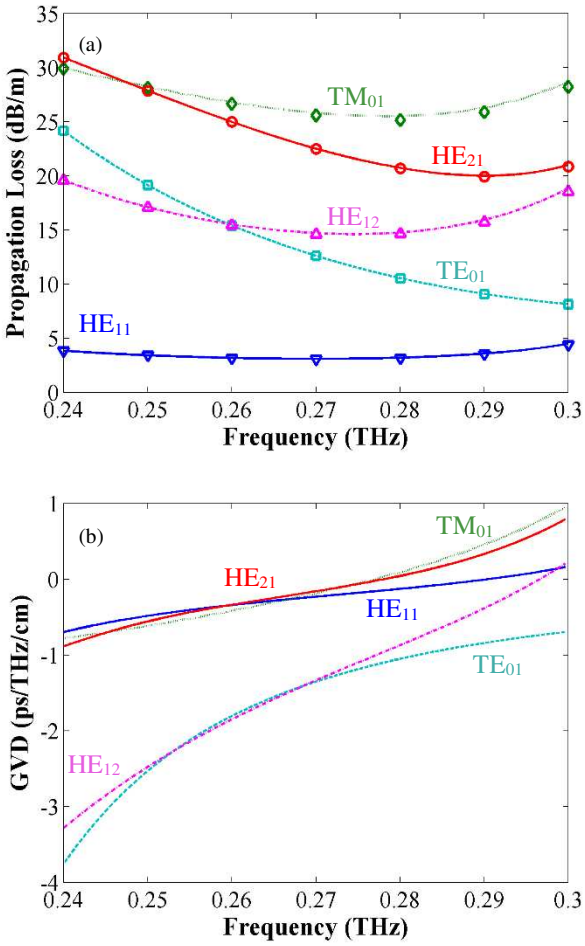

Fig. 4. (a) Propagation loss and (b) group velocity dispersion of the ideal Bragg fiber for the modes indicated in Fig. 3.

the radial photonic crystal structure, and is therefore confined within the fiber. The white areas show the regions where the TM/EH modes are confined within the fiber.

The highlighted region of Fig. 3(a), expanded in Fig. 3(b), designates the operating parameter range of interest for the designed THz Bragg fiber. In (b), the dispersion curves of the desired fundamental HE_{11} mode and other representative competing modes of the Bragg fiber, calculated by the transfer matrix method [44] and simulated by COMSOL, are overlaid onto the bandgap diagram. Here, both in the theoretical analysis and simulation, the outermost cladding layer was set to be an absorbing layer with no reflected wave from the outside. Such an arrangement is achievable in practice by using a thick and lossy shielding layer. As mentioned at the end of section II, the second-order bandgap was chosen as the operating band for the desired HE_{11} mode to overcome the fabrication challenges. According to the previous published work [42], the propagation losses of all modes in a Bragg fiber, including the five selected representative modes, are sensitive to, and indeed determined by, their relative positions to the bandgaps. The proposed Bragg fiber is thereby designed to exhibit large propagation loss discrimination between the desired HE_{11} mode and other competing modes over the frequency range of interest, creating a modal-filtering effect, as shown in Fig. 4(a), to obtain signal propagation with only the desired HE_{11} mode. Of course, at discontinuites and transitions the other modes may be excited, but the same is true of many well-developed waveguiding structures [45], and dealing with this issue will require further studies of specific cases.

Fig. 4(a) shows that the desired HE_{11} mode is the lowest loss propagation mode across the frequency range from 0.24 to 0.3 THz, and that the propagation loss of the main competing mode HE_{12} is at least ~4.3 times greater in dB/m than that of the HE_{11} mode. The propagation loss discrimination between HE_{11} and HE_{12} modes at the center of the band is greater than that at the edge of the band; at 0.27 THz, the propagation loss of the HE_{11} mode is 3.085 dB/m, while the propagation loss of HE_{12} is 14.7 dB/m. Note that, owing to the significant difference in polarization between HE_{11} and TE_{01}, there is barely any transfer from HE_{11} to TE_{01}. Therefore, TE_{01} is not the main competing

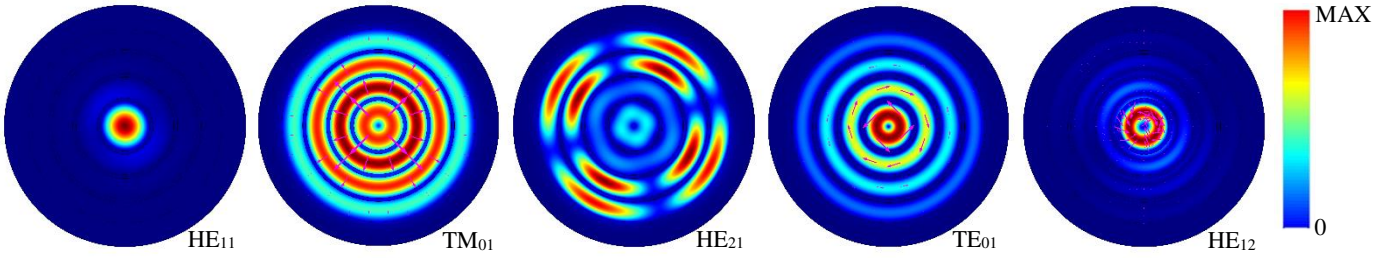

Fig. 5. Normalized electric field of the five selected representative modes at 0.27 THz. The field linearly decreases from red to blue. The magenta arrows in TM_{01}, TE_{01} and HE_{12} indicate the directions of the electric field.

mode of HE_{11}, although it is the second lowest loss mode at some frequencies. In addition, Fig. 4(b) shows that the desired HE_{11} mode exhibits low group velocity dispersion, with less than -0.56 ps/THz/cm between 0.246 to 0.276 THz. In Figs. 3 and 4, the consistency seen between our analytical theoretical analysis and the numerical COMSOL simulations validates the accuracy of both methods.

The normalized mode patterns of five selected representative modes are presented in Fig. 5. It can be seen that the electric field of the desired HE_{11} mode is well-confined within the low loss air core, while the mode patterns of the competing modes spread into the lossy cladding region, thus experiencing high signal attenuation. It is noted that the normalized mode patterns of the TE_{01} and TM_{01} mode appear similar to each other, but the direction of the electric field is radically different: the TE_{01} has circular E-field lines and the TM_{01} mode has radial ones. Also, the central peak in the normalized electric field of the HE_{12} mode is barely visible in Fig. 5, but closer inspection shows that the polarization and electric field components are similar to those of the ideal HE_{12} mode and very different to those of the TE_{01} and TM_{01} modes. Thus, we can still categorize it as the HE_{12} mode.

B. Eigenmode simulation of practical Bragg fiber with support bridges

The support bridges, which mechanically maintain the air gaps between dielectric layers, introduce additional EM-field leakage since they act as discontinuities in the photonic crystal, periodically perturbing its structure [42]. The support bridges also cause mode coupling between the guided mode in the core and the surface modes, resulting in a higher propagation loss [46]. However, the desired HE_{11} mode mainly propagates within the core region, and thereby the negative impact of the support bridges on the propagation loss of HE_{11} is relatively small compared to the other competing modes. Nevertheless, it is preferable to use thin support bridges and as few of them as possible to minimize their negative impact. Making use of the DLP rapid prototyping technology, only two bridges per air gap were necessary. Such a highly porous structure would be difficult to achieve with other thermal fabrication technologies owing to the deformation exhibited in the processing [7].

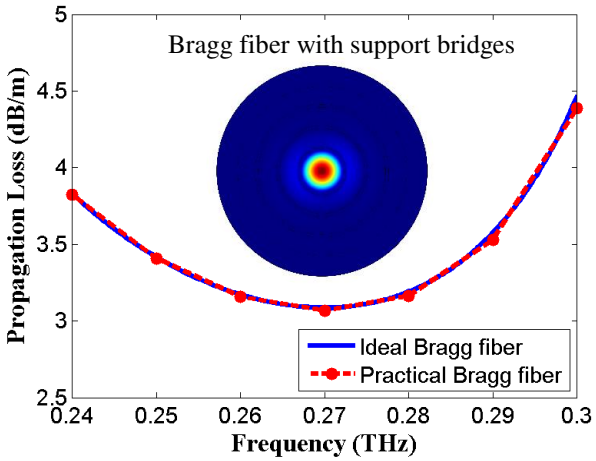

Fig. 6. Theoretical propagation losses of HE_{11} mode in ideal and practical Bragg fiber. The inset shows the normalized electric field of the HE_{11} mode in a practical Bragg fiber with support bridges.

The impact of the support bridges on the desired HE_{11} mode was investigated using the COMSOL eigenmode solver. A practical Bragg fiber with support bridges using the measured data listed in TABLE I was simulated. As shown in Fig. 6, the presence of the support bridges has negligible impact on the propagation loss of the desired HE_{11} mode, leading us to the conclusion that the negative impact of the support bridges on the propagation loss of the desired HE_{11} mode can be well suppressed provided only a very few support bridges are used, placed perpendicular to the polarization of the HE_{11} mode. Additionally, a high-porosity structure like this fiber is barely achievable using thermal fabrication techniques. The inset shows the mode pattern of the desired HE_{11} mode in this practical Bragg fiber with support bridges; note that the HE_{11} mode is well-confined in the air core, despite the presence of the support bridges.

C. Propagation simulation of the real Bragg fiber using practical geometry and material parameters

To verify that the fabricated Bragg fiber operates with asymptotically single-mode behavior, an electromagnetic simulation using the actual as-fabricated geometry and material parameters was carried out using CST Microwave Studio®. The set-up and the simulation results are shown in Fig. 7. The total length of the Bragg fiber was 30 mm. An open boundary was applied at the maximum and minimum plane of all directions. The fundamental HE_{11} mode of a hollow cylindrical metallic waveguide (HCMW) was used to feed the Bragg fiber from the left at x = -1.11 mm. x = 0 mm indicates the interface between the HCMW and the Bragg fiber. The mode profile in the Bragg fiber for a frequency of 0.27 THz at x = 1 mm and x = 30 mm are shown in Figs. 7(c) and 7(d), respectively, from which we

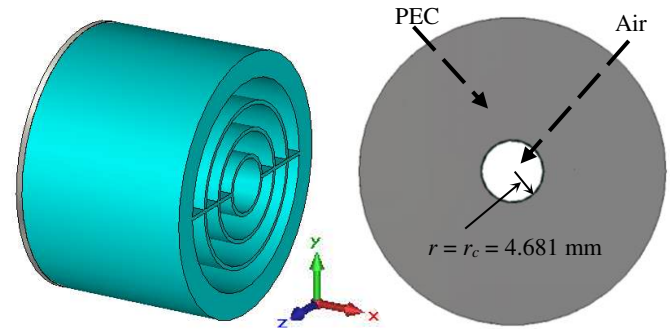

(a) Perspective view

(b) Circular waveguide feed x= -1.11 mm

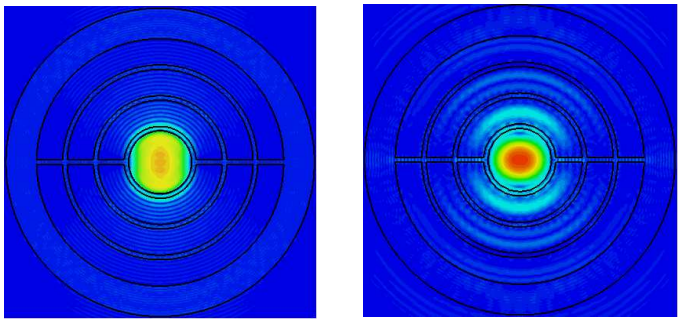

(c) Mode profile at x = 1 mm

(d) Mode profile at x = 30 mm

Fig. 7. Transmission simulation of the Bragg fiber using practical geometry and material parameters listed in TABLE I: (a) Perspective view of the setup of the transmission simulation; (b) HCMW feed at x = -1.11 mm; (c) Mode profile at x = 1 mm; (d) Mode profile at x = 30 mm.

can see that the mode profile at the front part of the Bragg fiber (x = 1 mm) is a superposition of multiple modes, but eventually the mode profile at the end of the Bragg fiber (x = 30 mm) becomes the desired HE_{11} mode. Therefore, the proposed Bragg fiber shows strong mode selectivity while allowing the wave to be transmitted in an asymptotically single-mode pattern.

IV. Measurement Results and Discussion

The measurement set-up used is shown in Fig. 8. The WR-3 rectangular waveguides (RWG) at both ends are on Oleson Microwave Labs (OML) 220 GHz to 325 GHz frequency extenders, which were connected to a Keysight PNA-X vector network analyzer. The left WR-3 RWG was connected to port 1 of the PNA-X, and the right WR-3 RWG to port 2. A circular corrugated horn antenna with rectangular waveguide input was mounted on each frequency extender. The EM wave emitted from the left horn antenna was collimated and focused onto the core of the Bragg fiber by a pair of parabolic mirrors. The Gaussian beam profile resulting coupled directly to the desired HE_{11} mode in the fiber. A 2D simulation of our 2-inch diameter 90° off-axis parabolic mirror using COMSOL gives the Gaussian beam waist w_0 at focal point of 3.19 mm, which is about 68.15% of the core radius r_c. Using mode-coupling theory for HCMW [47], the coupling coefficient between the free-space Gaussian beam and the desired HE_{11} mode in the proposed Bragg fiber is estimated to be 88%, thanks to the similar Bessel function patterns between the HE_{11} mode in

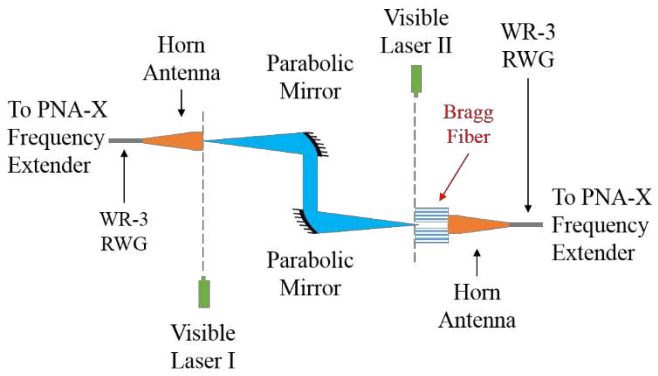

Fig. 8. Setup of the characterization experiment. The WR-3 rectangular waveguides at both ends were mounted on OML 220 GHz to 325 GHz frequency extenders which were connected to a Keysight PNA-X.

Bragg fiber and the TE_{11} mode in HCMW. The coupling coefficient into our proposed Bragg fiber is thus fundamentally high. The corrugated horn antenna on the right was placed on a movable stage to permit both alignment with the core at the output end of the Bragg fiber, and the measurement of the Bragg fibers of different lengths. Two auxiliary visible lasers were initially used to determine the focal points of the parabolic mirrors, aiding alignment.

The measured transmission coefficients of the 30 mm and 100 mm Bragg fibers are shown in Fig. 9(a). A standard LRL calibration was performed to shift the reference plane to the output ports of the WR-3 RWGs which were mounted on the frequency extenders, and then a cut-back calibration method [48] was used to calculate the propagation loss which removes the impact of coupling loss between the free-space Gaussian beam and the fiber. However, the cut-back method was not able to remove the systematic phase error caused by impedance mismatch in the transmission path, resulting in the fast ripple in the data. However, it should be noted that this frequency domain measurement approach is fundamentally accurate and, while the time domain measurements used for many reported THz waveguides may yield very smooth data, this is only because of the lower level of frequency resolution achievable. The IF bandwidth was set to 100 Hz, the averaging factor was 384, and 456 frequency points were recorded over the truncated frequency range of interest from 0.24 to 0.3 THz. The raw measurement data of the transmission coefficients for the two sample fibers are shown in Fig. 9(a).

To reduce the systematic phase error, a moving window average technique was applied to the raw measurement data of the transmission coefficients, shown in Fig. 9(b). In other words, the transmission coefficient at each frequency point is the mean value of its 11 nearest neighbor points (including itself), occupying about 2.2% aperture of the frequency range from 0.24 to 0.3 THz. Since the Bragg fiber is a passive component with no resonance peaks in the transmission spectrum, this technique is effective. Therefore, compared with the raw data in Fig. 9(a), the smoothed curves in Fig. 9(b) actually represent the average data of the transmission coefficients.

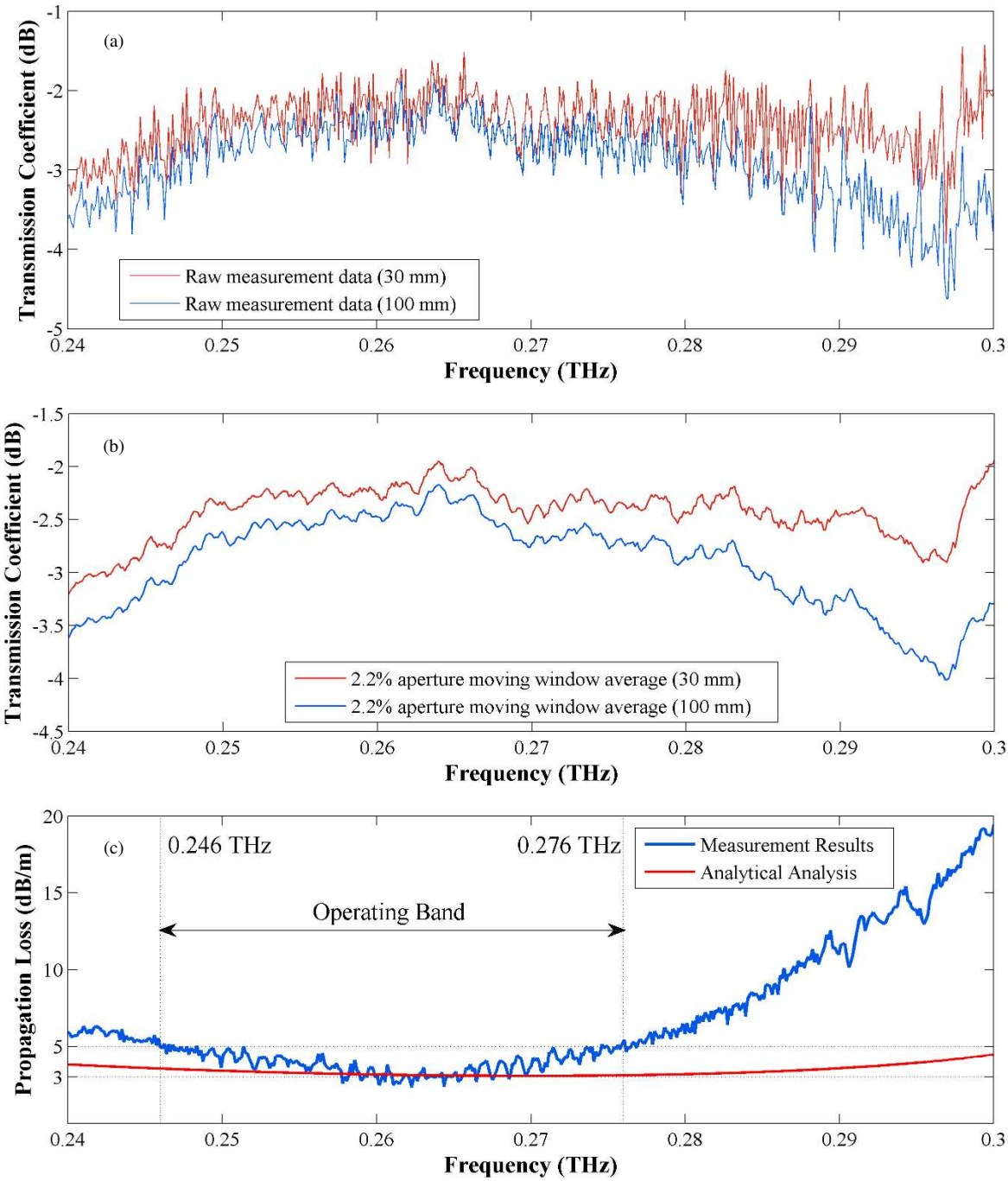

Fig. 9. Measurement results. (a) The raw measurement data of the transmission coefficients. (b) The moving window average of the transmission coefficients based on their raw values. (c) The measured propagation loss of the proposed Bragg fibers (blue line) and the analytical analysis result of the desired HE_{11} mode (red line).

Using the cut-back calibration method [48] and the average data of the transmission coefficients shown in Fig. 9(b), the measured propagation loss of the proposed Bragg fiber is shown in Fig. 9(c). The blue line shows the averaged measurement value of the propagation loss. Again, the residual fast ripple is still caused by impedance mismatches between components in the transmission path, which is not corrected out with a cut-back calibration. The red line shows the COMSOL simulated propagation loss for the HE_{11} mode of the fabricated Bragg fiber. The averaged measured data is in good agreement with the simulated propagation loss of the HE_{11} mode over the central frequency region from 0.246 to 0.276 THz. From 0.22 to 0.246 THz, and from 0.276 to 0.3 THz, the measured loss of the waveguide is much greater than the simulated HE_{11} result. This is believed to be due to mode transition between the desired HE_{11} mode and other higher order competing modes at these frequencies introduced by the higher propagation loss of the HE_{11} mode and the smaller loss discrimination. Nevertheless, a low average propagation loss, below 5 dB/m across the frequency range of interest from 0.246 to 0.276 THz, was achieved, with an average minimum of 3 dB/m at 0.265 THz.

TABLE II
REVIEW OF THZ MICROSTRUCTURED FIBERS

Reference No.	Minimum Propagation Loss (L_{min})		Propagation Loss (L) or Average Propagation Loss(L_{avg})		Material	Fabrication Technique
	Loss (dB/m)	Frequency (THz)	Loss (dB/m)	Frequency Range (THz)		
[16] ‡	= 1.3	= 0.24	L_{avg} < 34.72	0.2 ~ 0.35	Cylic-olefin Copolymer	Extrusion
[17]	= 30.38	= 0.105	30.38 < L_{avg} < 282.1	0.08 ~ 0.24	n/a	3D Printing
[18]*	= 4.34	≈ 0.27	4.34 < L_{avg} < 34.74	0.2 ~ 0.35	Stratasys® VeroWhitePlus	3D Printing
[19]*	≈ 51.6	≈ 0.17	51.6 < L < 151.9	0.145 ~ 0.207	Asiga® PlasClear	3D Printing
[20]†	= 12.16	= 0.69	12.16 < L < 130.29	0.1 ~ 2	PTFE & PMMA	Rolling
[21]*	= 30	= 0.375	30 < L < 250	0.29 ~ 0.47	PMMA	Drawing
[22]*	= 5	≈ 0.27	5 < L < 80	0.2 ~ 0.35	Zeonex	Drawing
[23] ‡	= 0.87	= 0.77	n/a	n/a	PTFE	Stacking
[24]†	≈ 156.35	≈ 1	L_{avg} = 260.58	0.65 ~ 1	PMMA	Stacking
[25] ‡	≈ 1	= 2.54	n/a	n/a	Silver & PS	Coating
[26]	< 6.95	= 0.88	L_{avg} < 9.99	0.78 ~1.02	TOPAS	Drilling & drawing
[27]	< 21.71	≈ 0.5	L_{avg} = 39.08±8.69	0.2 ~ 0.8	TOPAS	Drilling & drawing
[28]	≈ 43.43	≈ 0.3	43.43 < L < 173.72	0.2 ~ 1.2	Zeonex	Drilling & drawing
[29]†	< 5.21±4.34	= 0.249	L_{avg} < 130.29	0.05 ~ 0.5	LDPE	Molding & drawing
[30]	= 86.86	= 1.3	L_{avg} < 477.72	1 ~ 1.6	PMMA	Drilling
[31]	n/a	n/a	L < 217.15	> 0.6	HDPE	Stacking & fusing
This Work ‡	≈3 ‡	= 0.265	L_{avg} < 5	0.246 ~ 0.276	EnvisionTEC® HTM140	3D Printing

* Each of these papers reported a microstructured fiber with multiple transmission windows. Only the results of the closest transmission window compared to the frequency range of interest of this work (from 0.246 to 0.276 THz) are presented in this table.
† Each of these papers reported multiple designs of microstructured fibers. Only the result with lower loss from each publication is presented in this table.
‡ A detailed comparison between these low loss microstructured fibers can be found in sections I and IV.

A comparion of the reported experimental work on THz microstructured fibers is shown in TABLE II. Among the THz microstructured fibers listed, the work in [16] shows a lower minimum loss at similar frequency range, but its average propagation loss is higher than that of this work. Also, the THz microstructured fiber in [16] does not work in a single-mode pattern, while our proposed Bragg fiber is able to operate in an asymptotically single-mode pattern over the frequency range from 0.246 to 0.276 THz. We note that the dielectric-lined hollow cylindrical metallic waveguide in [25] exhibits lower loss at 2.54 THz and can enable quasi-single mode propagation by means of efficient coupling. However, due to the simplicity of its structure, it offers very limited degrees of freedom to optimize the loss discrimination between its desired mode and higher order competing modes, resulting in multimode interference which causes measurement difficulties, though much longer sample waveguide was used [25]. In contrast, the geometry of the proposed all-dielectric Bragg fiber offers a high degree of freedom to manipulate its photonic bandgap and dispersion curves, and it thereby allows the realization of low propagation loss of the desired mode and large loss discrimination between the desired mode and its competing modes simultaneously, resulting in strong mode selectivity.

V. CONCLUSIONS

In this paper we described the design and measured performance of a THz Bragg fiber, fabricated by digital light processing rapid prototyping, which provides low-loss guiding of THz waves. The Bragg fiber was measured with a free space measurement platform using a Keysight PNA-X and OML frequency extenders, and its propagation loss was extracted using the cut-back calibration method. The results show the average propagation loss of the proposed asymptotically single-mode Bragg fiber is less than 5 dB/m over the frequency from 0.246 to 0.276 THz, which is, to the best of our knowledge, the lowest loss asymptotically single-mode all-dielectric microstructured fiber yet reported in this frequency range, with an average minimum loss of 3 dB/m at 0.265 THz.

ACKNOWLEDGMENT

This work has been supported by the China Scholarship Council, the Thailand Research Fund through the TRF Senior Research Scholar Program with Grant No.RTA6080008 and the Royal Golden Jubilee Ph.D. Program with Grant No.PHD/0093/2557. The authors would like to thank Graham Brown, Joshua Freeman and Yunhua Zhang for helpful discussions. The samples were fabricated in the EPSRC National Facility for Innovative Robotic Systems. The data associated with this paper are openly available from the University of Leeds data repository [49].

REFERENCE

[1] P. H. Siegel, "THz instruments for space," *IEEE Transactions on Antennas and Propagation*, vol. 55 no. 11, pp. 2957-2965, Nov. 2007.
[2] P. H. Siegel, "Terahertz technology in biology and medicine," *IEEE transactions on microwave theory and techniques*, vol. 52, no. 10, pp. 2438-2447, Oct. 2004.
[3] T. Nagatsuma, G. Ducournau, and C. C. Renaud, "Advances in terahertz communications accelerated by photonics," *Nature Photonics*, vol. 10, no. 6, pp. 371-379, Jun 2016.
[4] A. G. Davies, A. D. Burnett, W. Fan, E. H. Linfield, and J. E. Cunningham, "Terahertz spectroscopy of explosives and drugs," *Materials today*, vol. 11, no. 3, pp. 18-26, Mar 2008.
[5] S. S. Dhillon, M. S. Vitiello, E. H. Linfield, et al. (43 more authors) "The 2017 Terahertz Science and Technology Roadmap," *Journal of Physics D: Applied Physics*, vol. 50, no. 4, pp. 043001, Jan. 2017.
[6] A. Argyros, "Microstructures in polymer fibers for optical fibers, THz waveguides, and fiber-based metamaterials," *ISRN Optics*, Feb. 2013.
[7] S. Atakaramians, S. Afshar, T. M. Monro, and D. Abbott,"Terahertz dielectric waveguides," *Adv. Opt. Photonics*, vol. 5, no. 2, pp. 169-215, Jun. 2013.

[8] T. Ito, Y. Matsuura, M. Miyagi, H. Minamide, and H. Ito, “Flexible terahertz fiber optics with low bend-induced losses,” *JOSA B*, vol. 24, no. 5, pp. 1230-1235, May 2007.
[9] C. D. Nordquist, M. C. Wanke, A. M. Rowen, C. L. Arrington, M. Lee, and A. D. Grine, “Design, fabrication, and characterization of metal micromachined rectangular waveguides at 3 THz,” In *2008 IEEE Antennas and Propagation Society International Symposium*. San-Diego, CA, 2008.
[10] I. Robertson, N. Somjit, and M. Chongcheawchamnan, *Microwave and Millimetre-Wave Design for Wireless Communications*. Hoboken, NJ, USA: Wiley, 2016.
[11] H. M. Heiliger, M. Nagel, H. G. Roskos, H. Kurz, F. Schnieder, W. Heinrich, R. Hey, and K. Ploog, “Low-dispersion thin-film microstrip lines with cyclotene (benzocyclobutene) as dielectric medium,” *Applied physics letters*, vol. 70, no. 17, pp. 2233-2235, Apr. 1997.
[12] M. Y. Frankel, S. Gupta, J. A. Valdmanis, and G. A. Mourou, “Terahertz attenuation and dispersion characteristics of coplanar transmission lines,” *IEEE Transactions on microwave theory and techniques*, vol. 39, no. 6, pp. 910-916, Jun. 1991.
[13] M. Bozzi, A. Georgiadis, and K. Wu, “Review of substrate-integrated waveguide circuits and antennas,” *IET Microwaves, Antennas & Propagation*, vol. 5, no. 8, pp. 909-920, Jun. 2011.
[14] L. Jin, R. M. A. Lee, and I. Robertson, “Analysis and design of a novel low-loss hollow substrate integrated waveguide,” *IEEE Transactions on Microwave Theory and Techniques*, vol. 62, no. 8, pp. 1616-1624, Aug. 2014.
[15] A. Argyros, "Microstructured polymer optical fibers," *J. Lightw. Technol.*, vol. 27, no. 11, pp. 1571-1579, Jun. 2009.
[16] *S. Atakaramians, S. Afshar V, M. Nagel, H. K. Rasmussen, O. Bang, T. M. Monro, and D.* Abbott, "Direct probing of evanescent field for characterization of porous terahertz fibers," *Appl. Phys. Lett.*, vol. 98, no. 12, p. 121104, Mar. 2011.
[17] Z. Wu, W. R. Ng, M. E. Gehm, and H. Xin, "Terahertz electromagnetic crystal waveguide fabricated by polymer jetting rapid prototyping," *Opt. Exp.*, vol. 19, no. 5, pp. 3962-3972, Feb. 2011.
[18] J. Yang, J. Zhao, C. Gong, H. Tian, L. Sun, P. Chen, L. Lin, and W. Liu, “3D printed low-loss THz waveguide based on Kagome photonic crystal structure,” *Opt. Exp.*, vol. 24, no, 20, pp. 22454-22460, Oct. 2016.
[19] J. Li, K. Nallappan, H. Guerboukha, and M. Skorobogatiy, “3D printed hollow core terahertz Bragg waveguides with defect layers for surface sensing applications” *Opt. Exp.*, vol. 25, no. 4, pp. 4126-4144, Feb. 2017.
[20] A. Dupuis, K. Stoeffler, B. Ung, C. Dubois, and M. Skorobogatiy, "Transmission measurements of hollow-core THz Bragg fibers," *JOSA B*, vol. 28, no. 4, pp. 896-907, Apr. 2011.
[21] V. Setti, L. Vincetti, and A. Argyros, "Flexible tube lattice fibers for terahertz applications," *Opt. Exp.*, vol. 21, no. 3, pp. 3388-3399, Feb, 2013.
[22] W. Lu, S. Lou, and A. Argyros, “Investigation of Flexible Low-Loss Hollow-Core Fibers With Tube-Lattice Cladding for Terahertz Radiation,” *IEEE Journal of Selected Topics in Quantum Electronics*, vol. 22, no. 2, pp. 214-220, Mar. 2016.
[23] J. Y. Lu, C. P. Yu, H. C. Chang, H. W. Chen, Y. T. Li, C. L. Pan, and C. K. Sun, "Terahertz air-core microstructure fiber," *Appl. Phys. Lett.*, vol. 92, no. 6, p. 064105. Feb 2008.
[24] J. Anthony, R. Leonhardt, S. G. Leon-Saval, and A. Argyros, "THz propagation in kagome hollow-core microstructured fibers," *Opt. Exp.*, vol. 19, no. 19, pp. 18470-18478, Sep. 2011.
[25] Mitrofanov, O., James, R., Fernández, F. A., Mavrogordatos, T. K. and Harrington, J. A., “Reducing transmission losses in hollow THz waveguides," *IEEE Transactions on Terahertz Science and Technology*, vol. 1, no. 1, pp. 124-132, Sep. 2011.
[26] H. Bao, K. Nielsen, H. K. Rasmussen, P.U. Jepsen, and O. Bang, "Fabrication and characterization of porous-core honeycomb bandgap THz fibers," *Opt. Exp.*, vol. 20, no. 28, pp. 29507-29517, Dec. 2012.
[27] K. Nielsen, H. K. Rasmussen, A. J. Adam, P. C. Planken, O. Bang, and P. U. Jepsen, "Bendable, low-loss Topas fibers for the terahertz frequency range," *Opt. Exp.*, vol. 17, no. 10, pp. 8592-8601, May 2009.
[28] J. Anthony, R. Leonhardt, A. Argyros, and M. C. Large, "Characterization of a microstructured Zeonex terahertz fiber". *JOSA B*, vol. 28, no. 5, pp. 1013-1018, May 2011.
[29] A. Dupuis, A. Mazhorova, F. Désévédavy, M. Rozé, and M. Skorobogatiy, "Spectral characterization of porous dielectric subwavelength THz fibers fabricated using a microstructured molding technique," *Opt. Exp.*, vol. 18, no. 13, pp. 13813-13828, Jun. 2010.
[30] C. S. Ponseca Jr, R. Pobre, E. Estacio, N. Sarukura, A. Argyros, M. C. Large, and M. A. van Eijkelenborg, "Transmission of terahertz radiation using a microstructured polymer optical fiber," *Opt. Lett.*, vol. 33, no. 9, pp. 902-904, May 2008.
[31] H. Han, H. Park, M. Cho, and J. Kim, "Terahertz pulse propagation in a plastic photonic crystal fiber," *Appl. Phys. Lett.*, vol. 80, no. 15, pp. 2634-2636, Apr 2002.
[32] L. Vincetti, “Empirical formulas for calculating loss in hollow core tube lattice fibers,” *Opt. Exp.*, vol. 24, no, 10, pp. 10313-10325, May 2016.
[33] L. Vincetti, “Single-mode propagation in triangular tube lattice hollow-core terahertz fibers,” *Optics Communications*, vol. 283, no. 6, pp. 979-984, Mar. 2010.
[34] P. Yeh, A. Yariv, and E. Marom, "Theory of Bragg fiber," *JOSA*, vol. 68, no. 9, pp. 1196-1201, Sep. 1978.
[35] P. Russell, “Photonic crystal fibers,” *Science*, vol. 299, no. 5605, pp. 358-362, Jan. 2003.
[36] F. Poletti, “Nested antiresonant nodeless hollow core fiber,” *Opt. Exp.*, vol. 22, no. 20, pp. 23807-23828, Oct. 2014.
[37] L. Vincetti, and V. Setti, “Waveguiding mechanism in tube lattice fibers,” *Opt. Exp.*, vol. 18, no, 22, pp. 23133-23146. Oct. 2010.
[38] M. D’Auria, W. J. Otter, J. Hazell, B. T. Gillatt, C. Long-Collins, N. M. Ridler, and S. Lucyszyn, “3-D printed metal-pipe rectangular waveguides,” *IEEE Transactions on Components, Packaging and Manufacturing Technology*, vol. 5, no. 9, pp. 1339-1349. Sep. 2015.
[39] K. Cook, G. Balle, J. Canning, L. Chartier, T. Athanaze, M. A. Hossain, C. Han, J. E. Comatti, Y. Luo,and G. D. Peng, “Step-index optical fiber drawn from 3D printed preforms,” *Optics Letters*, vol. 41, no. 19, pp. 4554-4557, Oct. 2016.
[40] W. D. Furlan, V. Ferrando, J. A. Monsoriu, P. Zagrajek, E. Czerwińska, and M. Szustakowski, “3D printed diffractive terahertz lenses,” *Optics letters*, vol. 41, no. 8, pp. 1748-1751, Apr. 2016.
[41] Z. Wu, M. Liang, W. R. Ng, M. Gehm, and H. Xin, “Terahertz horn antenna based on hollow-core electromagnetic crystal (EMXT) structure,” *IEEE Transactions on Antennas and Propagation*, vol. 60, no. 12, pp. 5557-5563, Dec. 2012.
[42] B. Hong, M. Swithenbank, N. Somjit, J. Cunningham, and I. Robertson, “Asymptotically single-mode small-core terahertz Bragg fiber with low loss and low dispersion,” *Journal of Physics D: Applied Physics*, vol. 50, no. 4, pp. 045104, Dec. 2016.
[43] A. Kitagawa, and J. I. Sakai, "Bloch theorem in cylindrical coordinates and its application to a Bragg fiber," *Phys. Rev. A.*, vol. 80, no. 3, p. 033802, Sep. 2009.
[44] S. Guo, S. Albin, and R. Rogowski, "Comparative analysis of Bragg fibers," *Opt. Exp.*, vol. 12, no. 1, pp. 198-207. Jan. 2004.
[45] D. Dai, Y. Tang, and J. E. Bowers, “Mode conversion in tapered submicron silicon ridge optical waveguides,” *Opt. Exp.*, vol. 20, no. 12, pp. 13425-13439, Jun. 2012.
[46] J. A. West, C. M. Smith, N. F. Borrelli, D. C. Allan, and K. W. Koch, "Surface modes in air-core photonic band-gap fibers," *Opt. Exp.*, vol. 12, no. 8, pp. 1485-1496, Apr. 2004.
[47] T. Ito, Y. Matsuura, M. Miyagi, H. Minamid, and H. Ito, “Flexible terahertz fiber optics with low bend-induced losses,” *JOSA B*, vol. 24, no. 5, pp. 1230-1235, May 2007
[48] J. C. Daly, *Fiber optics*. Boca Raton, Florida:CRC Press. 1984.
[49] B. Hong, M. Swithenbank, N. Greenall, R. Clarke, N. Chudpooti, P. Akkaraekthalin, N. Somjit, J. Cunningham, and I. Robertson. (2017). Data associated with ‘Low-Loss Asymptotically Single-Mode THz Bragg Fiber Fabricated by Digital Light Processing Rapid Prototyping’. University of Leeds. [Dataset]. Available: https://doi.org/10.5518/248

Binbin Hong (S’16) was born in Zhejiang, China, in 1990. He received the B.Sc. degree in physics and M.Sc. degree in plasma physics from the Sichuan University, Chengdu, China, in 2011 and 2014, respectively. He is currently working towards the Ph.D. degree at the University of Leeds, Leeds, U.K.

His research interests include millimetre-wave and terahertz circuits and device, lab-on-a-chip terahertz microfluidic sensing, and terahertz super-resolution near-field microscopy.

Matthew Swithenbank received the B.Eng. and M.Eng. degrees in electronic and electrical engineering from the University of Leeds, Leeds, U.K., in 2013. He is currently working toward the Ph.D. degree at the Institute of Microwaves and Photonics, University of Leeds.

His research interest includes terahertz spectroscopy in microfluidic systems.

Nicholas Greenall received the B.Eng. And M.Eng. degrees in electronic and electrical engineering from the University of Leeds, Leeds, U.K., in 2013. He is currently working toward the Ph.D. degree at the Institute of Microwaves and Photonics, University of Leeds.

His research interest includes signal processing of terahertz time domain spectroscopy.

Roland G. Clarke (M'04) was born in Huddersfield, U.K., in 1966. He received the B.Sc. degree from the University of Leeds, Leeds, U.K., in 2003.For several years he was responsible for the technical management of high-frequency research laboratories at the University of Leeds.

He is currently a Senior Teaching Fellow within the School of Electronic & Electrical Engineering, and a member of the Institute of Microwaves & Photonics at the University of Leeds. His research interests are principally concerned with high-frequency metrology, particularly millimeter-wave and submillimeter-wave vector network analyzer measurements.

Nonchanutt Chudpooti (S'16) received a first-class honors B.Sc. degree from the King Mongkut's University of Technology North Bangkok in 2012, where he is currently pursuing the Ph.D. degree supported by the Thailand Research Fund through the Royal Golden Jubilee Ph.D. Program.

His main research focuses on the application of microwave microfluidic sensors, millimeter-wave substrate integrated circuit applications and Substrate Integrated Waveguide (SIW) applications. He was a recipient of the Best Presentation Award and Young Researcher Encouragement Award at the Thailand-Japan Microwave in 2015 and 2016, respectively.

Prayoot Akkaraekthalin (M'98) received the B.Eng. and M.Eng. degrees in Electrical Engineering from King Mongkut's University of Technology North Bangkok (KMUTNB), Thailand, in 1986 and 1990, respectively, and the Ph.D. degree from the University of Delaware, Newark, USA, in 1998. From 1986 to 1988, he worked as a research and development engineer at the Microtek Company, Thailand. In 1988, he joined the Department of Electrical Engineering, KMUTNB.

His current research interests include RF/microwave circuits, wideband and multiband antennas, telecommunications, and sensor systems. Professor Prayoot is the author and co-author of over 40 international journals, over 200 conference papers, and 4 books/book chapters. He was the editor-in-chief for the ECTI Transactions between 2011 and 2013. He is a member of IEEE, IEICE Japan, ECTI and EEAAT Associations Thailand. He was the chairman for the IEEE MTT/AP/ED Thailand Joint Chapter from 2007 to 2010 and the vice president and the president of ECTI Association, Thailand from 2012 to 2013 and from 2014 to 2015, respectively. He is now the head of the Senior Research Scholar Project under the grant from Thailand Research Fund (2015-2017).

Nutapong Somjit (M'10) received the Dipl.-Ing. (MSc) degree from Dresden University of Technology in 2005 and the PhD degree from the KTH Royal Institute of Technology in 2012. Then, he returned to Dresden to lead a research team in micro-sensors and MEMS ICs for the Chair for Circuit Design and Network Theory. In 2013, he was appointed Lecturer (Assistant Professor) in the School of Electronic and Electrical Engineering, University of Leeds.

His main research focuses on RFICs, RF MEMS, tuneable antennas, and RFIC-MEMS integration. Dr Somjit was the recipient of the Best Paper Award (EuMIC prize) at the European Microwave Week in 2009. He was awarded a Graduate Fellowship from the IEEE Microwave Theory and Techniques Society (MTT-S) in 2010 and 2011, and the IEEE Doctoral Research Award from the IEEE Antennas and Propagation Society in 2012. In 2016, he was the Chair of the Student Design Competition for the European Microwave Week.

John E. Cunningham received the B.Sc. degree in physical sciences from University College London, London, U.K., in 1995, the M.Sc. degree from Imperial College London, London. U.K., in 1996, and the Ph.D. degree from the University of Cambridge, Cambridge, U.K. in 2000. He is now Professor of nanoelectronics and Deputy Head of the School of Electronic and Electrical Engineering at the University of Leeds, U.K and is director of the UK EPSRC network for terahertz science and technology, Teranet.

His research interests span many areas in high frequency science and technology, with an emphasis on picosecond-timescale measurement schemes.

Ian D. Robertson (F'12) received his BSc (Eng.) and PhD degrees from King's College London in 1984 and 1990, respectively. From 1984 to 1986 he worked in the GaAs MMIC Research Group at Plessey Research, Caswell. After that he returned to King's College, initially as a Research Assistant working on the T-SAT project and then as a Lecturer, leading the MMIC Research Team and becoming Reader in 1994. In 1998 he was appointed Professor of Microwave Subsystems Engineering at the University of Surrey, where he established the Microwave Systems Research Group and was a founder member of the Advanced Technology Institute. In June 2004 he was appointed to the Centenary Chair in Microwave and Millimetre-Wave Circuits at the University of Leeds. He was Director of Learning and Teaching from 2006 to 2011 and Head of School from 2011 to 2016. He was elected Fellow of the IEEE in 2012 in recognition of his contributions to MMIC design techniques and millimetre-wave system-in-package technology. He was General Technical Programme Committee Chair for the European Microwave Week in 2011 and 2016.